macromol

MDPI

Article

A Novel Acidic Polysaccharide Rich in Galactose and Galacturonic Acid from *Spatholobi caulis*: Structural Characterization and Anti-Aging Effects in *Caenorhabditis elegans*

Yuening Luo [1,†], Min Liang [1,†] and Dengfeng Yang [1,2,*]

[1] Guangxi Key Laboratory of Marine Natural Products and Combinatorial Biosynthesis Chemistry, Guangxi Academy of Marine Sciences, Guangxi Academy of Sciences, Nanning 530007, China
[2] College of Pharmacy, Guangxi University of Chinese Medicine, Nanning 530007, China
* Correspondence: dengfengyang@163.com
† These authors contributed equally to this work.

Abstract

Spatholobi caulis is considered an important medicinal plant in traditional Chinese medicine, which has the functions of promoting blood circulation, replenishing blood, enhancing immunity, and stimulating hematopoiesis, but its bioactive polysaccharides remain underexplored. In this study, stepwise ethanol precipitation of *Spatholobi caulis* yielded a water-soluble polysaccharide fraction, designated SCP-50, which was selected for further structural and functional characterization due to its relatively high yield and typical pectin-like monosaccharide composition. The structural features of SCP-50 were systematically investigated, and its anti-aging effects were evaluated using the *Caenorhabditis elegans* model. Structural analysis combining monosaccharide composition, methylation-GC-MS, and 1D/2D NMR spectroscopy suggested that SCP-50 is primarily composed of galactose (30.5%), galacturonic acid (29.4%), arabinose (20.1%), and rhamnose (11.1%), with a homogalacturonan backbone and branched arabinan/galactan side chains. In vivo assays with *C. elegans* demonstrated that SCP-50 (1.0 mg/mL) extended the mean lifespan by 31.3% and the median lifespan from 10 to 14 days, without affecting reproductive capacity. It also enhanced stress resistance by reducing intracellular ROS levels (15.4%), improving survival under oxidative stress (40.6% increase), and enhancing thermotolerance (18.8% improvement in motility recovery). SCP-50 increased the mRNA expression of *daf-16* (1.7-fold) and *skn-1* (2.5-fold), suggesting the involvement of these stress-responsive pathways. These findings demonstrate that SCP-50 exerts anti-aging effects potentially through coordinated regulation of oxidative stress resistance and longevity pathways, positioning it as a promising candidate for further investigation as a functional food ingredient or nutraceutical.

Keywords: *Spatholobi caulis*; polysaccharide; *Caenorhabditis elegans*; anti-aging; oxidative stress; structural characterization

Check for updates

Academic Editor: Rajendra Rohokale

Received: 20 August 2026
Revised: 24 September 2026
Accepted: 1 October 2026
Published: 3 October 2026

Copyright: © 2026 by the authors. Licensee MDPI, Basel, Switzerland. This article is an open access article distributed under the terms and conditions of the Creative Commons Attribution (CC BY) license.

1. Introduction

Aging is a universal biological process that predisposes individuals to a range of chronic diseases, including cardiovascular disorders, neurodegenerative conditions, and metabolic syndromes, posing a growing public health challenge worldwide [1,2]. Natural products derived from medicinal plants, particularly plant-derived polysaccharides,

have attracted increasing attention as promising sources of bioactive compounds due to their diverse bioactivities [3]. In particular, polysaccharides from Traditional Chinese medicine (TCM) have received considerably less attention than small-molecule components such as alkaloids and flavonoids [4–6]. Nevertheless, emerging evidence has revealed that these biopolymers exhibit intricate structures and diverse bioactivities, including immunomodulatory, antitumor, and antioxidant properties [7]. For instance, a polysaccharide isolated from *Asparagus cochinchinensis* potentiates innate immune memory through TLR4–MAPK signaling [8]; a polysaccharide derived from Danggui Buxue Decoction reprograms tumor-associated macrophages to enhance the chemotherapeutic efficacy of gemcitabine [9]; and *Polygonatum sibiricum* polysaccharide alleviates sarcopenia via the PI3K/Akt/mTOR axis [10]. The antioxidant capacity of natural polysaccharides has become a research hotspot due to its close association with oxidative stress-related disorders [11]. These advances underscore the promising potential of TCM polysaccharides as bioactive candidates and highlight the urgency of exploring under-investigated medicinal herbs.

The dried vine of *Spatholobus suberectus* Dunn, known as *Spatholobi caulis* (*S. caulis*), grows widely in southern China. In traditional medicine, it has been used to treat anemia, menstrual irregularities, and rheumatoid arthritis [12]. Modern pharmacological studies have corroborated these traditional applications, verifying the hematopoietic, anti-inflammatory, and analgesic effects of *S. caulis* extracts [13]. Its aqueous decoctions are widely used in folk medicine to invigorate Qi and nourish blood. Previous phytochemical investigations have identified diverse flavonoids, phenolic acids, and volatile oils in this herb [14,15]. Although a few polysaccharides from *S. caulis* have been reported with preliminary in vitro antioxidant activities [16], their detailed structural features and in vivo anti-aging activities remain largely unexplored.

Caenorhabditis elegans has emerged as a robust model for aging and oxidative stress research, owing to its short lifespan, genetic manipulability, and highly conserved stress-response signaling pathways [17]. A growing body of literature has demonstrated that multiple plant-derived polysaccharides prolong lifespan and enhance stress tolerance in *C. elegans*. For example, *Astragalus* polysaccharides exert beneficial effects via the DAF-16 pathway [18,19]; *Cyclocarya paliurus* polysaccharides function in a *skn-1*- and *hsf-1*-dependent manner [20]. Comparable bioactivities have also been documented for polysaccharides from *Ganoderma lucidum* [21], *Panax notoginseng* root [22], *Polygonatum cyrtonema Hua* [23], and *Rubus suavissmus* [24]. These findings validate the feasibility of employing *C. elegans* to assess the biological activities of *S. caulis* polysaccharides.

The biological functions of polysaccharides depend heavily on their structure. Molecular weight, monosaccharide composition, glycosidic linkage patterns, and molecular conformation collectively determine their bioactivities such as immunoregulation and antioxidant effects [25–27]. Thus, structural elucidation is a critical first step toward understanding the bioactivity of a given polysaccharide. Subtle structural variations can lead to distinct changes in biological performance [28]. However, the precise structural features of a highly branched acidic pectic polysaccharide from *S. caulis*, such as glycosidic linkage patterns and backbone architecture, remain to be elucidated, and its anti-aging activity has not been evaluated in vivo. In the present study, a homogeneous polysaccharide fraction from S. caulis, designated SCP-50, was isolated and structurally characterized, including its monosaccharide profile, glycosidic linkages, and molecular weight distribution. Subsequently, its antioxidant and anti-aging properties were systematically evaluated in *C. elegans* in vivo, with a focus on the potential involvement of the DAF-16 and SKN-1 pathways. This study thus adds to our understanding of *S. caulis* polysaccharides and supports the evidence-based application of this medicinal herb.

2. Materials and Methods

2.1. Chemicals and Reagents

S. caulis was purchased from Guangxi Medicinal Materials Market (Nanning, China). The material was identified by the College of Pharmacy, Guangxi University of Chinese Medicine, according to the monograph of *Spatholobi caulis* in the Chinese Pharmacopoeia (2020 Edition). A voucher specimen (accession number: GXKXYBB-20260825-1) was deposited at the specimen museum of the Institute of Biology, Guangxi Academy of Sciences. Monosaccharide standards (mannose (Man), rhamnose (Rha), arabinose (Ara), galactose (Gal), glucose (Glc), galacturonic acid (GalA), and glucuronic acid (GlcA)) and pullulan standards were obtained from Shanghai Yuanye Biotechnology Co., Ltd. (Shanghai, China). Trifluoroacetic acid (TFA), 1-phenyl-3-methyl-5-pyrazolone (PMP), deuterium oxide (D_2O, 99.9 atom% D), 5-fluoro-2′-deoxyuridine (FudR), and 2′,7′-dichlorofluorescein diacetate (DCF-DA) were purchased from Sigma-Aldrich (St. Louis, MO, USA). Sodium chloride (NaCl), agar, tryptone, cholesterol, calcium chloride ($CaCl_2$), and magnesium sulfate ($MgSO_4$) were purchased from Sangon Biotech Co., Ltd. (Shanghai, China); DMSO was purchased from Macklin Co., Ltd. (Shanghai, China); Sodium hydroxide (NaOH), chloroform, and anhydrous sodium sulfate were purchased from Xilong Scientific Co., Ltd. (Shenzhen, China); Iodomethane (CH_3I) were purchased from Aladdin Co., Ltd. (Shanghai, China); Sodium thiosulfate, acetic acid, acetic anhydride, dichloromethane, sodium borohydride, and 4 Å molecular sieves were purchased from Tianjin Kermel Chemical Reagent Co., Ltd. (Tianjin, China); Sodium borodeuteride ($NaBD_4$) were purchased from Leyan Co., Ltd. (Shanghai, China); Perchloric acid, ethanol, methanol, and ethyl acetate were purchased from Chengdu Kelong Chemical Co., Ltd. (Sichuan, China); RNA extraction reagent (Iso-plus) and SYBR Green master mix were purchased from Takara Bio Inc. (Kusatsu, Japan); all primers used in this study were synthesized by GeneCreate Biological Engineering Co., Ltd. (Wuhan, China).

2.2. Extraction and Purification of SCP-50

S. caulis was pulverized into powder and defatted by soaking in 95% ethanol (1:20, *w*/*v*) at room temperature for 2 days. The extracted solution was centrifuged at 6000 rpm for 20 min to remove the supernatant containing fat-soluble components, and the residue was re-extracted under the same conditions. This process was repeated three times to ensure complete removal of lipophilic components. The residue was air-dried and then extracted with distilled water (1:15, *w*/*v*) at 80 °C for 4 h. After centrifugation (4000 rpm, 15 min), the supernatant was collected and concentrated under reduced pressure. Crude polysaccharides were precipitated by stepwise addition of ethanol. Ethanol was added to the concentrated solution to a final concentration of 40% (*v*/*v*) and kept overnight at 4 °C. The precipitate was collected by centrifugation (designated as SCP-40). Ethanol was then added to the resulting supernatant to reach a final concentration of 50% (*v*/*v*) and kept overnight at 4 °C. The precipitate was collected by centrifugation, redissolved in distilled water, and lyophilized to yield the polysaccharide fraction designated SCP-50.

2.3. Structural Characterization of SCP-50

2.3.1. Determination of Molecular Weight

The homogeneity and molecular weight of SCP-50 were determined by high-performance gel permeation chromatography (HPGPC) according to previously described methods with slight modifications [29]. Briefly, SCP-50 was dissolved in 0.1 M $NaNO_3$ solution to a concentration of 2.0 mg/mL and filtered through a 0.22 μm membrane. Analysis was performed on a Shodex OHpsk SB-806M HQ column (8.0 mm × 300 mm) (Shodex, Tokyo, Japan) maintained at 40 °C, with 0.1 M $NaNO_3$ as the mobile phase at a flow rate of

1.0 mL/min. The injection volume was 20 µL. The molecular weight was calculated using a calibration curve constructed with pullulan standards of known molecular weights (6.4, 9.8, 21.9, 49.4, 107, 218, 354, and 692 kDa).

2.3.2. Determination of Monosaccharide Composition

The monosaccharide composition of SCP-50 was determined by high-performance anion exchange chromatography with pulsed amperometric detection (HPAEC-PAD) following acid hydrolysis with slight modifications [30]. Briefly, SCP-50 (2 mg) was placed in a hydrolysis vial, and 1 mL of 2 M trifluoroacetic acid (TFA) was added. The vial was sealed and incubated at 121 °C in an oven for 2 h. After hydrolysis, the mixture was cooled to room temperature. An equal volume of methanol (1 mL) was added, and the solution was evaporated to dryness under a stream of nitrogen. This methanol addition and evaporation step was repeated three times to completely remove residual TFA. The hydrolysate was then dissolved in 1.20 mL of purified water, filtered through a 0.22 µm membrane, and analyzed by HPAEC-PAD. Separation was performed on a DionexCarboPac^{TM}PA20 (3mm × 150 mm) (Thermo Scientific, Waltham, MA, USA) at 30 °C with an electrochemical detector. The chromatographic separation was performed at a flow rate of 0.4 mL/min using a ternary gradient system consisting of the following mobile phases: solvent A (ddH_2O), solvent B (50 mM NaOH/100 mM Sodium Acetate), and solvent C (200 mM NaOH). The elution program was set as described in Table S1. Monosaccharides were identified and quantified by comparison with authentic standards of eleven monosaccharides: mannose (Man), ribose (Rib), rhamnose (Rha), glucuronic acid (GlcA), galacturonic acid (GalA), glucose (Glc), galactose (Gal), xylose (Xyl), arabinose (Ara), fucose (Fuc), and fructose (Fru).

2.3.3. FT-IR Spectroscopy

For FT-IR analysis, dried SCP-50 powder was placed directly onto the ATR crystal of a Nicolet iS10 FT-IR spectrometer (Thermo Scientific, Waltham, MA, USA). The spectrum was recorded in the frequency range of 4000–500 cm^{-1} with 32 scans at a resolution of 4 cm^{-1}.

2.3.4. Scanning Electron Microscopy (SEM) and Atomic Force Microscopy (AFM)

SEM and AFM were performed with reference to the method reported by Song with modifications [31]. For SEM observation, dried SCP-50 powder was mounted onto a conductive adhesive tape and sputter-coated with gold for 45 s. Images were captured using a FEI Quattro S scanning electron microscope (Thermo Fisher Scientific, Waltham, MA, USA) at an accelerating voltage of 3 kV. For AFM analysis, SCP-50 was dissolved in ultrapure water to a final concentration of 10 µg/mL and sonicated for 5 min. A drop of the solution was deposited onto a freshly cleaved mica sheet and air-dried at room temperature for 30 min, and imaging was carried out in tapping mode using a Dimension Icon atomic force microscope (Bruker, Ettlingen, Germany).

2.3.5. Methylation Analysis

Glycosidic linkage patterns of SCP-50 were determined by methylation analysis according to the method described by Pettolino with slight modifications [32]. Prior to methylation, SCP-50 was subjected to carboxyl reduction to convert uronic acids to their corresponding neutral sugars. The reduced product was dissolved in anhydrous DMSO and methylated with CH_3I in the presence of NaOH. The methylated polysaccharide was hydrolyzed with 2 M TFA at 121 °C for 4 h, reduced with $NaBH_4$, and acetylated with acetic anhydride/pyridine. The resulting partially methylated alditol acetates (PMAAs) were dissolved in dichloromethane and analyzed by GC-MS (Agilent 6890N-5975C, Santa Clara, CA, USA) equipped with an HP-5MS column (30 m × 0.32 mm, 0.25 µm). The temperature

program was: 50 °C held for 1 min, increased to 130 °C at 50 °C/min, then to 230 °C at 3 °C/min, and held for 10 min. Helium was used as the carrier gas at a flow rate of 1.0 mL/min. The injector temperature was 250 °C, and the injection volume was 1 µL. Mass spectra were recorded in electron ionization (EI) mode with a scan range of m/z 40–500. PMAAs were identified by their retention times and mass spectra compared with literature data. The relative molar percentages of PMAAs were calculated by normalizing the total peak area of all identified PMAAs to 100% for each sample (SCP-50 and SCP-50R).

2.3.6. Nuclear Magnetic Resonance (NMR) Spectroscopy

NMR analysis was performed with reference to the method reported by Yao with modifications [33]. For NMR analysis, freeze-dried SCP-50 was dissolved in 1 mL of D_2O (99.9 atom% D) and lyophilized. This process was repeated twice to exchange labile protons. The sample was then redissolved in 0.55 mL of D_2O and transferred to a 5 mm NMR tube. All NMR spectra were recorded on an Agilent 800 MHz NMR spectrometer (Agilent Technologies, Santa Clara, CA, USA) equipped with a cryoprobe at 25 °C. One-dimensional (^{1}H and ^{13}C) and two-dimensional (^{1}H-NMR, ^{13}C-NMR, ^{1}H-^{1}H COSY, ^{1}H-^{13}C HSQC-edited, ^{1}H-^{13}C HMBC, ^{1}H-^{1}H NOESY, ^{1}H-^{1}H HSQC-TOCSY) spectra were acquired. Chemical shifts were referenced to the HDO signal (δH 4.79 ppm). Data were processed using MestReNova software 14.0.0 (Mestrelab Research, Santiago de Compostela, Spain). Monosaccharide residues were assigned based on their ^{1}H and ^{13}C chemical shifts, in combination with monosaccharide composition and methylation analysis results. The glycosidic linkage sequences between residues were deduced from HMBC and NOESY correlations.

2.4. Radical Scavenging Capacity In Vitro

DPPH radical-scavenging capacity was measured as described by Blois [34]. Briefly, SCP-50 solution (20 µL, 0.125–2.0 mg/mL) was mixed with 180 µL DPPH solution (40 µg/mL in ethanol). After 30 min incubation in the dark at room temperature, absorbance was measured at 517 nm. Ascorbic acid was used as a positive control. Scavenging rate (%) = $(A_0 - A_1)/A_0 \times 100$, where A_0 and A_1 are the absorbances of the blank and sample, respectively. ABTS and T-AOC assays were carried out following the manufacturer's instructions (Solarbio, Beijing, China).

2.5. Caenorhabditis Elegans Assays

2.5.1. *C. elegans* Strains and Maintenance

Wild-type N2 nematodes were obtained from the Caenorhabditis Genetics Center (University of Minnesota, Minneapolis, MN, USA). Worms were maintained at 20 °C on nematode growth medium (NGM) plates seeded with *E. coli OP50* as a food source. Age-synchronized populations were obtained by hypochlorite treatment of gravid hermaphrodites as described by Furuhashi [35].

2.5.2. Lifespan Assay

The lifespan assay was performed as described by Chang with modifications [36]. Briefly, Synchronized L4 worms were cultured on NGM plates containing SCP-50 (0, 0.5, 1.0, 2.0 mg/mL) mixed with *E. coli OP50* at 20 °C. FudR (50 µM) was added at 72 h to inhibit progeny production, with 96 h designated as Day 0. At Day 0, 10 worms per group were transferred to fresh plates containing the corresponding SCP-50 concentrations. FudR was re-added on Days 2, 4, and 6. Worms were transferred to fresh plates every 2 days and scored daily for survival until all worms died. Worms that failed to respond to gentle prodding were scored as dead. Survival curves were plotted using the Kaplan–Meier method. At least 30 age-synchronized L4 worms were used per group per replicate, and

the assay was performed in three independent biological replicates. Data are presented as mean ± SD from three independent biological replicates. Statistical significance was assessed by the log-rank test.

2.5.3. Intracellular ROS Assay

Intracellular ROS levels were measured using the fluorescent probe DCF-DA [37]. Synchronized L1 larvae were cultured on NGM plates containing SCP-50 (0, 0.5, 1.0, 2.0 mg/mL) mixed with *E. coli OP50* at 20 °C for 96 h. Adult worms (day 4) were collected and incubated with 50 µM DCF-DA in M9 buffer at room temperature for 1 h in the dark. After incubation, the supernatant was removed, and the worms were treated with 10% ethanol for 10 min. Fluorescence images were captured using a fluorescence microscope (Keyence, Osaka, Japan) and quantified using ImageJ 1.54f (National Institutes of Health, Bethesda, MD, USA) software.

2.5.4. Fat Accumulation Assay

Fat accumulation was measured as described by Stuhr with modifications [38]. Briefly, Synchronized L1-stage N2 worms were cultured on NGM plates containing SCP-50 (0, 0.5, 1.0, 2.0 mg/mL) at 20 °C for 96 h. Adult worms (day 4) were collected, fixed in 4% paraformaldehyde, and stained with Nile Red (1 µg/mL) for 10 min. Fluorescence images were captured using a fluorescence microscope and quantified using ImageJ software.

2.5.5. Heat Stress Tolerance Assay

Synchronized L1-stage N2 worms were cultured on NGM plates containing SCP-50 (0, 0.5, 1.0, 2.0 mg/mL) mixed with *E. coli OP50* at 20 °C for 96 h. After treatment, adult worms (day 4) were collected for subsequent assays.

Thermotolerance was assessed as described previously with slight modifications [39]. Briefly, age-synchronized adult worms (day 4) were transferred to fresh NGM plates seeded with *E. coli OP50* and incubated at 35 °C. Survival was scored at 0, 6, and 10 h after the temperature shift.

Motility recovery was assessed as described previously [40]. Briefly, age-synchronized adult worms (day 4) were transferred to fresh NGM plates without *E. coli OP50* and incubated at 35 °C for 4 h (defined as 0 h). Worms were then returned to 20 °C for recovery. At 0, 6, and 12 h post-stress, thrashing movements were counted for 15 s in S-basal buffer. A control group was maintained at 20 °C throughout the experiment.

2.5.6. Quantitative Real-Time PCR (qRT-PCR)

qRT-PCR was measured as described by Furuhashi with minor modifications [35]. Briefly, total RNA was extracted from approximately 1000 age-synchronized adult worms (day 4) using RNAiso Plus (Takara, Kusatsu, Japan) according to the manufacturer's instructions. RNA concentration and purity were determined by absorbance at 260/280 nm using a NanoDrop spectrophotometer (Thermo Scientific, Waltham, MA, USA). First-strand cDNA was synthesized from 1 µg of total RNA using the PrimeScript RT reagent kit with gDNA Eraser (Takara, Kusatsu, Japan). qRT-PCR was performed on a qTOWER3 thermal cycler (Analytik Jena, Jena, Germany) using THUNDERBIRD SYBR qPCR Mix (Toyobo, Osaka, Japan). The cycling conditions were: 95 °C for 30 s, followed by 40 cycles of 95 °C for 5 s and 60 °C for 30 s. Melt curve analysis was performed to verify primer specificity. Relative gene expression was calculated using the $2^{-\Delta\Delta Ct}$ method with *act* as the internal control. Three independent biological replicates were performed for each gene, with each replicate consisting of approximately 1000 age-synchronized worms, and

technical triplicates were included in each qPCR run. Primer sequences used are listed in Table S2.

2.6. Statistical Analysis

All experiments were performed in at least three independent replicates. Data are expressed as mean ± standard deviation (SD). Statistical comparisons between two groups were performed using Student's *t*-test. For multiple group comparisons, one-way analysis of variance (ANOVA) followed by Dunnett's post hoc test was applied. Lifespan assays were analyzed using the Kaplan–Meier method and log-rank test. Differences were considered statistically significant at $p < 0.05$. All statistical analyses were performed using GraphPad Prism software 10.1.2 (GraphPad Software, San Diego, CA, USA).

3. Results

3.1. Isolation and Purification of SCP-50

Among the fractions obtained by graded ethanol precipitation (40–80%), the 50% ethanol precipitate exhibited the highest yield (22.45% of the crude polysaccharide) and was water-soluble, whereas the 40% fraction was insoluble and the 60–80% fractions had insufficient yields for further analysis. Therefore, this fraction was selected for further investigation based on its relatively high yield and water solubility and was designated SCP-50 for subsequent structural characterization and bioactivity assays. The structural characterization included HPGPC (molecular weight), GC-MS (glycosidic linkages), FT-IR (functional groups), SEM & AFM (surface morphology), and NMR (structural elucidation). The bioactivity assays included ROS measurement, fat accumulation, stress tolerance, lifespan, and RT-PCR analysis. The extraction and purification procedure is illustrated in Figure 1.

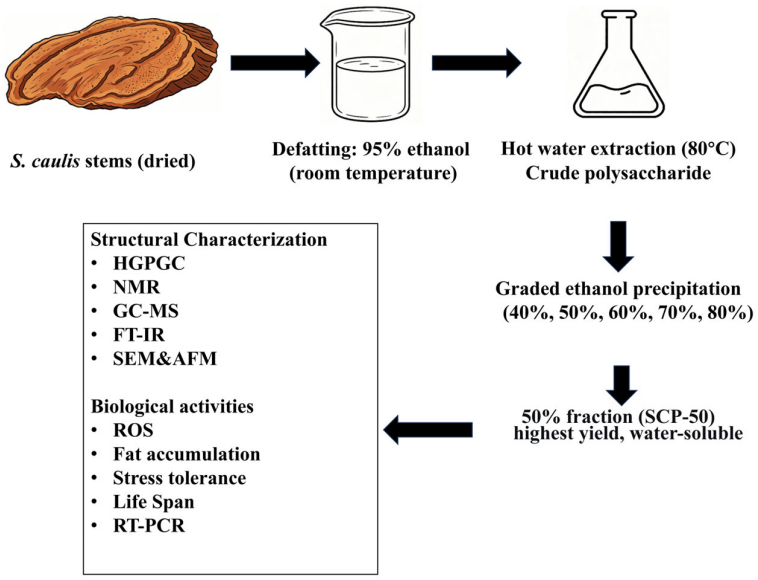


Figure 1. Extraction and purification procedure of SCP-50. The dried stems of *S. caulis* were defatted with 95% ethanol, followed by hot water extraction. The crude polysaccharide was then subjected to graded ethanol precipitation (40–80%). The 50% ethanol fraction (designated SCP-50) showed the highest yield and was selected for further studies.

3.2. Molecular Weight and Monosaccharide Composition

The molecular weight of SCP-50 was determined by HPGPC. As shown in Figure 2A, SCP-50 exhibited a single symmetrical peak at 8.70 min, indicating its homogeneity. Based on the pullulan standard curve, the molecular weight was calculated to be 64.7 kDa.

Monosaccharide composition analysis (Figure 2B) revealed that SCP-50 is mainly composed of galactose (30.5%), galacturonic acid (29.4%), arabinose (20.1%), and rhamnose (11.1%), with smaller amounts of glucose (1.9%), xylose (2.4%), mannose (0.6%), and fucose (1.2%), as well as glucuronic acid (2.8%). The high content of galacturonic acid classifies SCP-50 as an acidic polysaccharide.

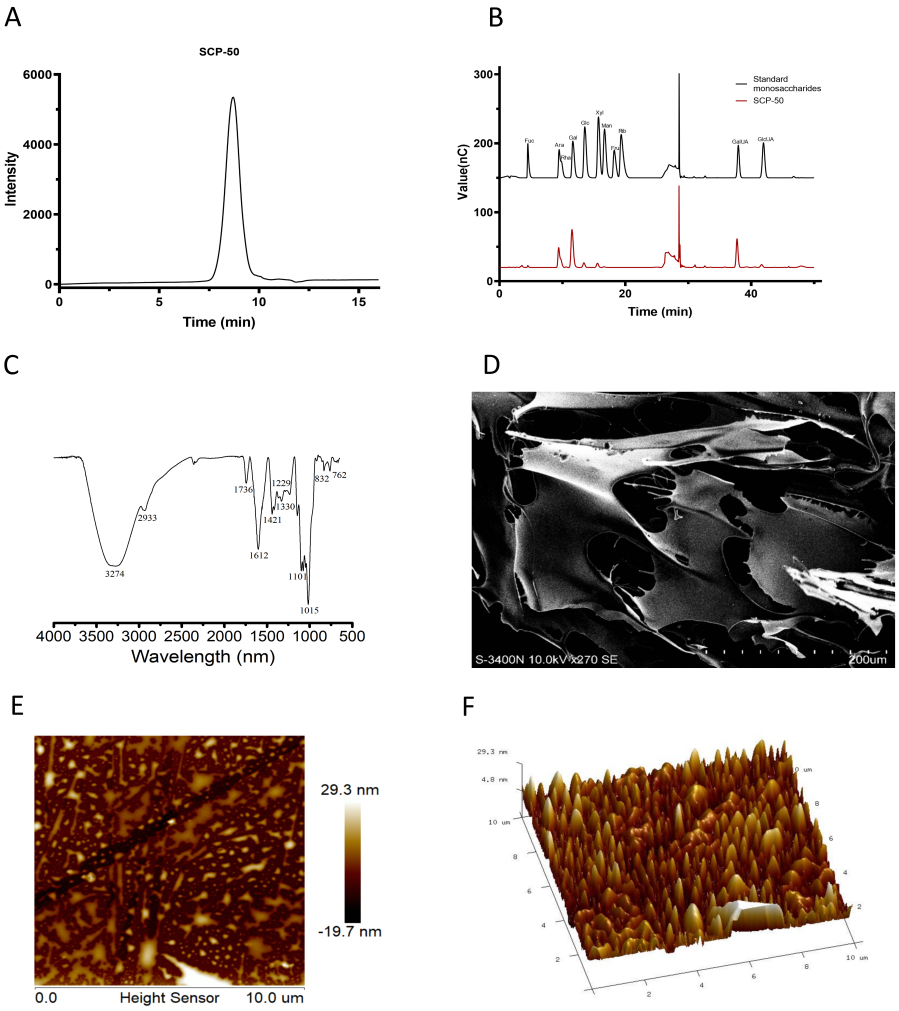


Figure 2. Structural characterization and surface morphology of SCP−50. (**A**) HPGPC chromatograms; (**B**) the monosaccharide composition of SCP−50; (**C**) the FT−IR spectra of SCP−50; (**D**) SEM image; (**E**) AFM height image (2D) of SCP−50; (**F**) AFM three-dimensional topographic image of SCP−50.

3.3. Structural Characterization

The FT-IR spectrum of SCP-50 (Figure 2C) revealed characteristic absorption bands at 1736 cm^{-1}, attributed to O-acetyl C=O stretching, and at 1612 cm^{-1}, assigned to free carboxylate moieties of uronic acids [34]. A weak peak was also observed at 832 cm^{-1}, which may be tentatively assigned to α-glycosidic linkages [35]; however, FT-IR alone is not sufficient to establish glycosidic configurations. This assignment was further supported by NMR analysis. The galacturonic acid content (29.4%) was independently determined by monosaccharide composition analysis.

SEM imaging (Figure 2D) showed that SCP-50 exhibited a hybrid structure composed of network-like and sheet-like domains, with a rough, honeycomb-patterned surface containing numerous irregular pores. AFM analysis (Figure 2E) further revealed that the

molecular chains of SCP-50 tended to aggregate into compact assemblies, with individual chain heights ranging from 4–5 nm and larger aggregates reaching approximately 10 nm.

The triple-helix conformation of SCP-50 was examined using the Congo red assay. As shown in Figure S1, the SCP-50–Congo red complex did not exhibit a significant red-shift in maximum absorption wavelength with increasing NaOH concentration, indicating the absence of a stable triple-helix structure.

3.4. Glycosidic Linkage Analysis

The glycosidic linkage patterns of SCP-50 were elucidated by methylation analysis coupled with GC-MS. The identified PMAAs are summarized in Table 1, and the total ion chromatogram is shown in Figure S2. Methylation analysis revealed that SCP-50 is a branched heteropolysaccharide with a moderate degree of branching, as evidenced by the substantial proportions of terminal residues (44.23%) and branch-point residues (22.41%), giving a terminal-to-branch ratio of 1.97, suggesting that the number of branching sites is roughly equivalent to that of terminal residues.

Table 1. Partially methylated alditol acetates (PMAAs) analysis of SCP-50.

Methylated Sugar	Mass Fragments (*m*/*z*)	Ratio %		Type of Linkage
		SCP-50	SCP-50R	
2,3,5-Me3-Ara	59,71,87,101,117,129,145,161	13.35	6.21	Araf-(1 → *
2,3,4-Me3-Fuc	59,71,89,101,117,131,143,149,161,175,187	16.79	1.69	Fucp-(1→
2,3-Me2-Xyl	59,71,87,101,117,129,131,146,161,173,189,206,233	15.25	5.30	→4)-Xylp-(1→
2,3-Me2-Ara	55,59,71,87,99,117,129,141,149,161,173,189	3.42	0.68	→5-Araf-(1→
2,3,4,6-Me4-Glc	59,71,87,101,117,129,145,161,173,191,205	-	0.71	Glcp-(1→
2,3,4,6-Me4-Gal	59,71,87,101,117,129,145,161,173,191,205	14.09	5.11	Galp-(1→
2-Me-Fuc	57,71,87,99,101,117,129,145,173,189,201,231,275	0.82	0.73	→3,4)-Fucp-(1→
2-Me-Xyl	71,85,99,117,129,143,159,161,171,191,203,261	0.98	1.17	→3,4)-Xylp-(1→
2-Me-Ara	74,87,99,117,127,143,159,173,187,201,217,233,261	1.95	2.28	→3,5)-Araf-(1→
3-Me-Rha	59,71,87,101,129,143,159,173,189,203,232	8.34	3.32	→2,4)-Rhap-(1→
2,3,6-Me3-Gal	55,59,71,87,101,117,129,143,161,173,189,203,233	2.85	53.59	→4)-Galp-(1→
2,3,6-Me3-Glc	59,71,87,101,117,129,131,149,161,173,189,203,233	7.73	10.46	→4)-Glcp-(1→
2,4,6-Me3-Man	57,71,85,101,117,129,143,161,173,203,217,234,277	4.13	0.89	→3)-Manp-(1→
2,6-Me2-Gal	71,87,99,117,129,143,159,189,203,217,233,261,305	-	4.45	→3,4)-Galp-(1→
2,3-Me2-Gal	55,71,85,101,117,127,142,159,201,231,261,305	10.32	3.39	→4,6)-Galp-(1→

* The linkage types are expressed as →X)-Galp-(1→, where the arrows indicate the linkage positions between glycosyl residues and X indicates the carbon position of the galactosyl residue involved in the glycosidic linkage.

Among the identified linkages, →4)-Galp-(1→ was the most abundant, accounting for 53.59% of the total. Upon carboxyl reduction, galactose increased markedly from 27.26% to 66.54%, and glucose from 7.73% to 11.18%, while other neutral sugars decreased proportionally. These increases are consistent with the conversion of galacturonic acid and glucuronic acid to their corresponding neutral sugars upon reduction, which is in agreement with the detection of uronic acids in the monosaccharide composition analysis (Figure 2B). Thus, the backbone of SCP-50 is likely composed primarily of a homogalacturonan domain, with possible occasional GlcA insertions.

Other linkages such as →4)-Xylp-(1→ and Araf-(1→ were also detected. Other identified residues included Galp-(1→, Fucp-(1→, →5)-Araf-(1→, →3,4)-Fucp-(1→, →3,4)-Xylp-(1→, →3,5)-Araf-(1→, →2,4)-Rhap-(1→, →3)-Manp-(1→, →3,4)-Galp-(1→, and →4,6)-Galp-(1→, which may contribute to the branched side chains of SCP-50. Among these, arabinose and galactose residues were relatively abundant, broadly consistent with the monosaccharide composition results (Figure 2B), suggesting the presence of branched arabinan and galactan domains in SCP-50.

After carboxyl reduction, the proportion of →4)-Galp-(1→ increased markedly from 2.85% to 53.59%, confirming the conversion of galacturonic acid to galactose upon reduction.

The normalized percentages of other linkages, such as Araf-(1→ and →5)-Araf-(1→, decreased accordingly. This does not mean these residues were lost during reduction. Rather, the sharp increase in galactose-derived PMAAs simply diluted the relative abundance of all other linkages in the normalized dataset.

3.5. NMR Analysis

The structure of SCP-50 was further characterized using nuclear magnetic resonance (NMR) spectroscopy. The ^{1}H and ^{13}C NMR spectra displayed characteristic resonances corresponding to methyl groups of rhamnose/fucose residues (δH 1.25–1.31, δC 17.6–17.8) and O-acetyl substituents (δH 2.08–2.18, δC 21.4–21.7) (Figure 3A,B). A carbon signal at δC 54.02 was assigned to methyl esters of uronic acids, whereas the signal at δC 176.63 verified the occurrence of galacturonic and glucuronic acids [41,42].

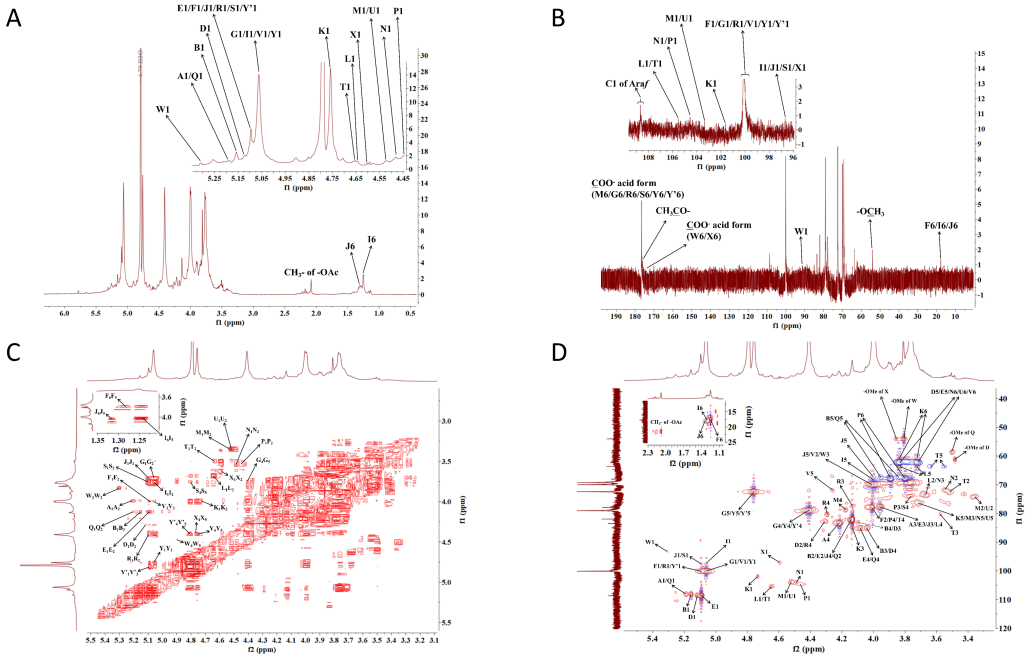


Figure 3. NMR spectra of SCP −50. (**A**) ^{1}H NMR spectrum; (**B**) ^{13}C NMR spectrum; (**C**) ^{1}H −^{1}H COSY spectrum; (**D**) ^{1}H −^{13}C HSQC spectrum.

Combining monosaccharide composition, methylation analysis, and two-dimensional NMR spectra (COSY, HSQC, HMBC, and NOESY), the chemical shifts of individual sugar residues were assigned. Anomeric signals in the region δH/δC 4.45–5.31/93.2–108.6 were observed, consistent with the presence of both α- and β-glycosidic linkages. The dominant anomeric signal at δ 5.09/108.62 was attributed to terminal α-L-Araf-(1→ residues, while signals at δ 5.19/108.17 and δ 5.15/108.17 were assigned to →5)-α-L-Araf-(1→ units. Signals corresponding to galactose and galacturonic acid residues, which constitute the major backbone components, were observed at δ 4.45–4.64/103.9–105.5, consistent with β-configurations. The signal at δ 4.74/101.97 was assigned to →3)-β-D-Manp-(1→ based on the characteristic H2 chemical shift (δH 3.99) of mannose [43]. Glycosidic linkage sequences were elucidated via COSY and HSQC correlations (Figure 3C,D). Key correlations, such as B H1/P H4 (δ 5.15/4.00) and B H1/P C4 (δ 5.15/77.92), confirmed the presence of →5)-α-L-Araf-(1→4,6)-β-D-Galp-(1→ linkages. Complete NMR assignments are compiled in Table S5.

Taken together, based on the combined methylation and NMR data, SCP-50 is proposed to be a branched pectic polysaccharide with a homogalacturonan backbone,

rhamnose-rich branch points, and complex arabinan/galactan side chains, along with O-acetyl substitutions.

3.6. Biological Activity

3.6.1. Radical-Scavenging Capacity

The radical-scavenging capacity of SCP-50 was evaluated using DPPH, ABTS, and total antioxidant capacity (T-AOC) assays. SCP-50 exhibited dose-dependent radical scavenging activity in all assays. In the DPPH assay, SCP-50 showed 31.98% scavenging at 1.0 mg/mL and 42.95% at 2.0 mg/mL. At 2.0 mg/mL, the scavenging rate was significantly higher than that of the crude polysaccharide (25.70%, $p < 0.01$) (Figure 4A). SCP-50 also demonstrated strong ABTS radical scavenging activity, reaching 91.07% at 2.0 mg/mL, comparable to the positive control VC (98.46% at 0.2 mg/mL) (Figure S3A). In the T-AOC assay, SCP-50 achieved 9.53 μmol/mL at 6.0 mg/mL, approaching the activity of VC (9.69 μmol/mL at 1.0 mg/mL) (Figure S3B).

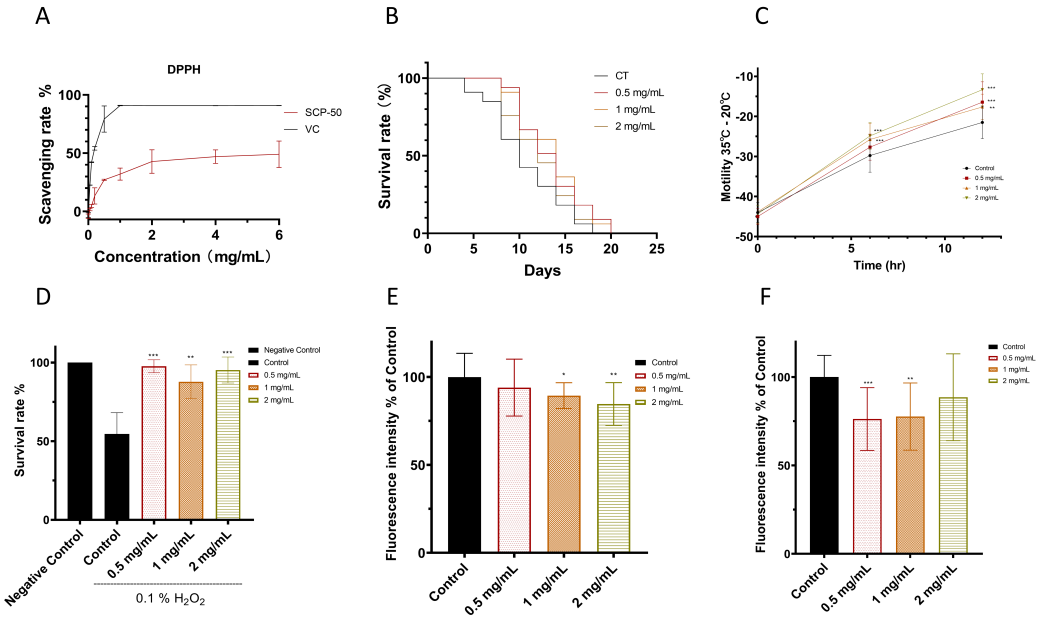


Figure 4. Antioxidant and anti-aging activities of SCP−50. (**A**) DPPH radical scavenging activity. (**B**) Lifespan curves of *C. elegans*. (**C**) Motility recovery after heat stress (35 °C, 4 h). Thrashing movements were counted at 0, 6, and 12 h post−stress. (**D**) Survival rate under 0.1% H_2O_2 oxidative stress. (**E**) Intracellular ROS levels measured by DCF−DA fluorescence. (**F**) Fat accumulation measured by Nile Red staining. Data are presented as mean ± SD. * $p < 0.05$, ** $p < 0.01$, *** $p < 0.001$ vs. Control.

3.6.2. Lifespan Extension and Stress Resistance

SCP-50 significantly extended the lifespan of *C. elegans*. At 1.0 mg/mL, the mean lifespan was extended by 31.3% (from 10.48 to 13.76 days), and the median lifespan increased from 10 to 14 days ($p < 0.001$, log-rank test; Table S3). Data were obtained from three independent biological replicates, with at least 30 animals per group per replicate. The maximum lifespan also increased from 18 days (control) to 20 days (Figure 4B). Treatment with SCP-50 at concentrations of 0.5, 1.0, and 2.0 mg/mL did not significantly affect the brood size or hatching rate compared to the control group (Figure S4), indicating that the observed longevity extension was not achieved at the expense of reproductive capacity. This decoupling of lifespan extension from fecundity suggests that SCP-50 may act through stress-resistance pathways such as DAF-16 or SKN-1, rather than through metabolic trade-offs [44–46].

Motility recovery after heat stress was enhanced by SCP-50 treatment. After 4 h heat stress (35 °C), the SCP-50 group showed 11.56% and 18.8% improvements in recovery rate at 6 h and 12 h post-stress, respectively (Figure 4C). Under the same heat stress conditions, SCP-50 also improved the survival rate after 6 h exposure (Figure S5). Under oxidative stress induced by 0.1% H_2O_2, SCP-50 pretreatment markedly increased survival, with the 2.0 mg/mL group achieving 95.23% survival versus 54.60% in the control after 1 h (Figure 4D). Additionally, SCP-50 reduced ROS accumulation by 15.35% and decreased fat accumulation by 23.75% (Figure 4E,F).

3.6.3. Real-Time PCR Analysis

To elucidate the molecular mechanisms underlying the anti-aging effects of SCP-50, the expression levels of key genes involved in stress resistance and longevity were examined by qRT-PCR. As shown in Figure 5, SCP-50 treatment significantly upregulated the expression of antioxidant enzymes, including sod-1 (1.9-fold), sod-2 (7.3-fold), ctl-1 (1.7-fold), and ctl-2 (2.0-fold). The remarkable 7.3-fold induction of sod-2, a mitochondrial superoxide dismutase, suggests a preferential effect on mitochondrial antioxidant defense. Furthermore, SCP-50 upregulated the transcription factors daf-16 (1.7-fold) and skn-1 (2.5-fold), suggesting that its anti-aging effects may involve the transcriptional upregulation of these stress-responsive pathways.

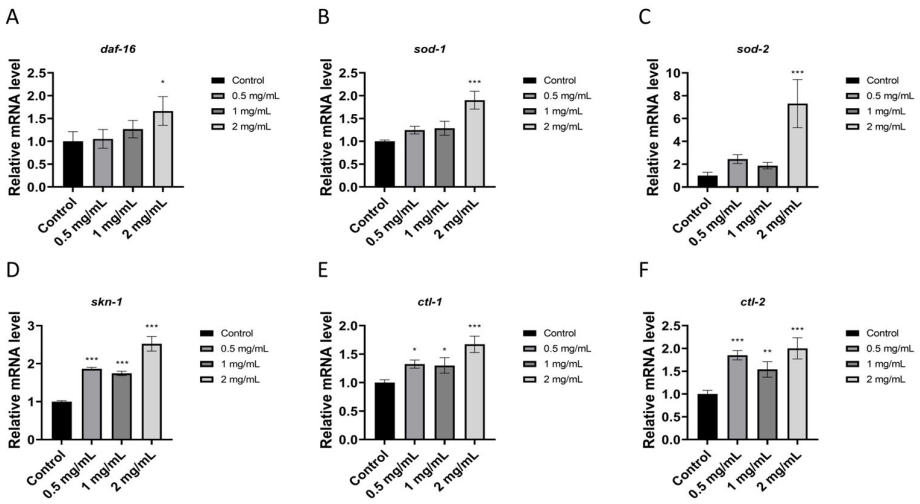


Figure 5. Effects of SCP-50 on gene expression in *C. elegans*. (**A**) *daf-16*; (**B**) *sod-1*; (**C**) *sod-2*; (**D**) *skn-1*; (**E**) *ctl-1*; (**F**) *ctl-2*. Data are presented as mean ± SD. * $p < 0.05$, ** $p < 0.01$, *** $p < 0.001$ vs. Control.

4. Discussion

Compared with the previously reported MDP1 (139.5 kDa, 26.1% uronic acid) from *S. caulis* [16], SCP-50 has a lower molecular weight (64.7 kDa), and a higher uronic acid content (29.4%). The total sugar content and protein content of SCP-50 were determined to be 77.5% and 5.8%, respectively (Table S4). Its HPGPC profile exhibited a single symmetrical peak, suggesting that SCP-50 is a relatively homogeneous fraction, which is typical for plant-derived polysaccharides, and its monosaccharide composition featured a more complex neutral sugar profile. The presence of uronic acids provides electrophilic groups for hydrogen donation, while the lower molecular weight increases the density of accessible terminal reducing groups per unit mass, both of which typically enhance radical scavenging activity [47–49]. The FT-IR data support this: the band at 1736 cm^{-1} corresponds to O-acetyl C=O stretching, and the band at 1612 cm^{-1} confirms free carboxylate moieties from uronic acids, which are the active sites for metal chelation and hydrogen donation. A weak peak was observed at 832 cm^{-1}, which may be tentatively assigned to α-glycosidic

linkages [50]; however, FT-IR alone is not sufficient to establish glycosidic configurations. This assignment was further supported by NMR analysis, in which the anomeric proton signals at δ 5.0–5.2 ppm confirmed the presence of α-linked galacturonic acid residues. The galacturonic acid content (29.4%) was independently determined by monosaccharide composition analysis.

SEM and AFM results indicate that SCP-50 has a porous and agglomerative morphology. Individual chains are between 4 and 5 nm in height, while larger aggregates can reach nearly 10 nm. The porous structure observed in the solid state may reflect the aggregation organization pattern of the SCP-50 chain, which may affect its hydrophilicity and solubility in aqueous media. Similar structures have also been reported in the antioxidant polysaccharide RRP-4 derived from Rhodiola rosea, which affects antioxidant activity through physical methods such as increasing surface area and exposing more active sites [51]. Of course, based on this morphological similarity alone, it cannot be concluded that SCP-50 also has the same antioxidant mechanism. Whether the solid-state properties of SCP-50 are directly related to the radical scavenging activity observed in solution requires further experimental verification. According to the literature [52], glucuronic acid and carboxyl group content are generally positively correlated with antioxidant activity. The glucuronic acid content provides the material basis for antioxidant activity [53], while the carboxyl group is directly involved in free radical scavenging through mechanisms such as hydrogen donation and chelation of metal ions [54,55]; neutral sugars such as galactose, fucose, and mannose may function by participating in hydrogen bond breakage through their hydroxyl groups [48]. On this basis, the antioxidant activity of SCP-50 may originate from the synergistic effect of glucuronide, carboxyl group, and porous morphology, with an auxiliary contribution from the hydroxyl group of neutral sugars. In addition, the Congo red test ruled out the possibility that SCP-50 has a triple helix structure, suggesting that its antioxidant activity may not depend on the ordered helix conformation.

The methylation data provided additional structural clues. The →4)-Galp-(1→ linkage made up 53.59% of the total after carboxyl reduction, along with →2,4)-Rhap-(1→ (8.34%) and →4,6)-Galp-(1→ (10.32%), pointing to a homogalacturonan backbone with branched arabinan and galactan side chains, together with rhamnogalacturonan-I (RG-I) domains.

Similar pectic structures have been reported for other bioactive plant polysaccharides. For instance, a pectic polysaccharide WSMP-A2b (37 kDa) isolated from Swertia mileensis also possesses a homogalacturonan backbone with arabinan and galactan side chains, and its antioxidant activity was partially attributed to its galacturonic acid content [56]. Similarly, a low-methoxyl pectin from Cicer arietinum husk (CAP, 105 kDa, 69% GalA) exhibited 29% DPPH scavenging activity at 1.0 mg/mL, which was also attributed to its high galacturonic acid content [57]. It should be noted that the DPPH and ABTS assays used in this study are chemical methods that measure radical-scavenging capacity rather than direct antioxidant activity in vivo.

Although SCP-50 had a lower GalA content than CAP, it exhibited a DPPH scavenging rate of 31.98% at 1.0 mg/mL, slightly higher than that of CAP (29%) under the same conditions [57]. Furthermore, SCP-50 showed a much higher ABTS scavenging rate of 91.07% at 2.0 mg/mL, indicating a strong electron-donating capacity. These results suggest that the antioxidant activity of SCP-50 is not solely dependent on galacturonic acid content but may also be attributed to its moderate degree of branching (22.41%) and the presence of arabinan and galactan side chains, which could enhance its conformational flexibility and accessibility to free radicals. While a branched structure with a homogalacturonan backbone is typical of pectins, the specificity of SCP-50 lies in its combination of a relatively low molecular weight, moderate branching, and distinct arabinan/galactan side chains. This unique structural combination may underlie its distinct bioactivity compared with

conventional pectins. Given that *S. caulis* is a widely used traditional Chinese medicine with abundant resources, SCP-50 may serve as a promising candidate for further development as a functional food ingredient or anti-aging agent.

The effective concentrations of SCP-50 in these chemical assays were higher than those of vitamin C, which is expected given that polysaccharides are macromolecules with lower molar activities. However, whether these concentrations are physiologically achievable requires further pharmacokinetic evaluation.

In *C. elegans*, SCP-50 extended the mean lifespan by approximately 31.3% at 1.0 mg/mL without affecting reproductive capacity, suggesting that lifespan extension was not simply a trade-off with fecundity. This pattern suggests the involvement of stress-response pathways, although a contribution from metabolic regulation cannot be excluded [44–46]. Furthermore, a significant reduction in Nile Red staining intensity was observed in the SCP-50-treated group, indicating that SCP-50 modulates fat storage in *C. elegans*. Given the complex relationship between lipid metabolism and longevity in this model, the functional significance of this change remains to be determined.

The qRT-PCR results are consistent with this interpretation. SCP-50 upregulated *daf-16* (1.7-fold) and *skn-1* (2.5-fold), along with downstream effectors *sod-1* (1.9-fold), *sod-2* (7.3-fold), *ctl-1* (1.7-fold), and *ctl-2* (2.0-fold). The strong induction of *sod-2*, which encodes a mitochondrial superoxide dismutase, suggests a particular impact on mitochondrial antioxidant defense, which is notable given the recognized role of mitochondrial ROS in aging.

Unlike many reported polysaccharides, *Lonicera japonica* polysaccharides (LJPs) and *Cremastra appendiculata* polysaccharides have been reported to primarily involve DAF-16, while *Tremella fuciformis* polysaccharides (TFLP) mainly affect metabolic pathways [58–60]. SCP-50 upregulated both *daf-16* and *skn-1* at the transcriptional level. This dual upregulation may help explain the 95.23% survival rate under acute oxidative stress (0.1% H_2O_2), versus 54.60% in controls. Since DAF-16 and SKN-1 control overlapping but distinct downstream gene sets involved in antioxidant defense, protein homeostasis, and detoxification, their combined upregulation may contribute to broader protection than either pathway alone. These results suggest that SCP-50 may act through coordinated regulation of oxidative stress resistance and metabolic homeostasis, supporting its potential for further investigation in anti-aging research. Whether SCP-50 directly engages upstream regulators of these pathways, and whether similar effects hold in mammals, remain open questions.

It should be noted that the selection of SCP-50 for in-depth investigation was based on its relatively high yield and typical pectin-like monosaccharide composition (dominated by GalA and Gal), rather than on a systematic activity screening of all ethanol-precipitated fractions (e.g., SCP-30 and SCP-70). Although this strategy is commonly adopted in polysaccharide isolation studies, it represents a limitation of the present work, as other fractions with superior or complementary activities cannot be ruled out. Future studies should include systematic comparative evaluations of fractions with different degrees of branching and methylation to better elucidate the structure–activity relationships of *Spatholobi caulis* polysaccharides. In addition, the concentrations used in the *C. elegans* assays are relatively high, and translation to mammalian systems would require careful dose optimization. The present findings should be considered preliminary and restricted to the nematode model.

5. Conclusions

We have isolated and systematically characterized SCP-50, a novel pectic polysaccharide from *S. caulis*. SCP-50 features a homogalacturonan backbone with branched arabi-

nan/galactan side chains, a relatively high uronic acid content (29.4%), and a molecular weight of 64.7 kDa. These structural attributes, particularly the abundant carboxyl groups and porous aggregated morphology, may contribute to its radical-scavenging activity.

In *C. elegans* assays, SCP-50 demonstrated significant anti-aging effects, extending mean lifespan by 31.3% without compromising reproductive fitness. Mechanistically, SCP-50 upregulated the transcriptional expression of *daf-16* and *skn-1* target genes, accompanied by upregulated antioxidant enzyme expression (*sod-1*, *sod-2*, *ctl-1*, *ctl-2*), reduced ROS accumulation, and enhanced resistance to oxidative and thermal stress. This dual-pathway upregulation distinguishes SCP-50 from many previously reported plant polysaccharides that act through a single pathway. However, since only mRNA-level changes were detected, the involvement of DAF-16 and SKN-1 was demonstrated only at the transcriptional level, and further validation through protein phosphorylation or nuclear translocation assays is needed.

Collectively, these findings suggest that SCP-50 may serve as a candidate for further investigation as a functional ingredient, although extensive toxicological and mammalian studies are still required.

6. Patents

No patents have been issued or applied for that are directly related to the results of this study.

Supplementary Materials: The following supporting information can be downloaded at: https://www.mdpi.com/article/10.3390/macromol6040093/s1, Figure S1: Changes in Congo red SCP-50 complex with various NaOH concentrations; Figure S2: GC-MS total ion chromatogram of PMAAs derived from SCP-50. (A) Before carboxyl reduction; (B) After carboxyl reduction; Figure S3: Antioxidant activities of SCP-50. (A) ABTS; (B) T-AOC; Figure S4: Reproductive capacity of *C. elegans* after treatment with SCP-50. Data are expressed as a percentage relative to the control group (mean ± SD). (A) Brood size; (B) Hatching rate. ns indicates no significant difference ($p > 0.05$); Figure S5: Survival rate of *C. elegans* under heat stress (35 °C). Survival was scored at 0, 6, and 10 h. Data are presented as mean ± SD; Table S1. Elution program for HPAEC-PAD analysis; Table S2: Primer sequences used in the analysis of gene expression; Table S3: Effects of SCP-50 on the lifespan of *C. elegans*; Table S4: Total sugar and protein contents of SCP-50; Table S5: Complete NMR assignments.

Author Contributions: Y.L.: writing—original draft, visualization, methodology, data curation, formal analysis, conceptualization. M.L.: data curation, formal analysis. D.Y.: funding acquisition, supervision. All authors have read and agreed to the published version of the manuscript.

Funding: This research was funded by the financial support from the National Natural Science Foundation of China (Grant No. 32360227 and 32360244), the Natural Science Foundation of Guangxi Province (2025GXNSFBA069375), the Guangxi Young Talents Development Program (2024-GXQMRCJH-03), and Basic Science and Research Foundation of Guangxi Academy of Sciences (CQ-C-202302, 2024YWE2113 and 2024YWE2114).

Institutional Review Board Statement: Not applicable.

Data Availability Statement: The original contributions presented in this study are included in the article/Supplementary Material. Further inquiries can be directed to the corresponding author.

Conflicts of Interest: The authors declare no conflicts of interest.

Abbreviations

The following abbreviations are used in this manuscript:

PMAAs	Partially methylated alditol acetates
AFM	Atomic force microscopy
DPPH	2,2-Diphenyl-1-picrylhydrazyl
FT-IR	Fourier transform infrared spectroscopy
HPGPC	High-performance gel permeation chromatography
HPAEC-PAD	High-performance anion exchange chromatography with pulsed amperometric detection
ROS	Reactive oxygen species
SEM	Scanning electron microscopy
T-AOC	Total antioxidant capacity
TFA	Trifluoroacetic acid

References

1. Tenchov, R.; Sasso, J.M.; Wang, X.; Zhou, Q.A. Aging Hallmarks and Progression and Age-Related Diseases: A Landscape View of Research Advancement. *ACS Chem. Neurosci.* **2024**, *15*, 1–30. [CrossRef]
2. Xi, J.Y.; Zhao, J.G.; Li, X.Q.; Yan, B.; Bai, J.J.; Xiang, Y.N.; Hu, W.; Hu, J.; Liao, Y.; Gu, J.; et al. Quantifying the loss of healthy life expectancy due to population ageing: Health benefit estimation from a global perspective. *BMJ Glob. Health* **2025**, *10*, e018194. [CrossRef]
3. Ma, X.; Zhao, B.; Zhang, J.; Wang, S.; Li, G.; Huang, Y.; Liang, Q.; He, J.; Xiao, Y.; He, J. Natural plant polysaccharides: Structural characteristics, biological activities, and recent advances in food applications. *Food Sci. Biotechnol.* **2026**, *35*, 2437–2453. [CrossRef]
4. Zou, B.; Long, Y.; Gao, R.; Liu, Q.; Tian, X.; Liu, B.; Zhou, Q. Nanodelivery system of traditional Chinese medicine bioactive compounds: Application in the treatment of prostate cancer. *Phytomedicine* **2024**, *135*, 155554. [CrossRef]
5. Cao, X.; Wang, Y.; Chen, Y.; Zhao, M.; Liang, L.; Yang, M.; Li, J.; Peng, M.; Li, W.; Yue, Y.; et al. Advances in traditional Chinese medicine for the treatment of chronic obstructive pulmonary disease. *J. Ethnopharmacol.* **2023**, *307*, 116229. [CrossRef]
6. Song, L.; Zhang, W.; Tang, S.-Y.; Luo, S.-M.; Xiong, P.-Y.; Liu, J.-Y.; Hu, H.-C.; Chen, Y.-Q.; Jia, B.; Yan, Q.-H.; et al. Natural products in traditional Chinese medicine: Molecular mechanisms and therapeutic targets of renal fibrosis and state-of-the-art drug delivery systems. *Biomed. Pharmacother.* **2024**, *170*, 116039. [CrossRef]
7. Zhang, H.; Li, Y.; Fu, Y.; Jiao, H.; Wang, X.; Wang, Q.; Zhou, M.; Yong, Y.-C.; Liu, J. A structure-functionality insight into the bioactivity of microbial polysaccharides toward biomedical applications: A review. *Carbohydr. Polym.* **2024**, *335*, 122078. [CrossRef]
8. Xie, X.-D.; Tang, M.; Yi, S.-L.; He, Y.; Chen, S.-Y.; Zhao, Y.; Chen, Q.; Cao, M.-X.; Yu, M.-L.; Wei, Y.-Y.; et al. Polysaccharide of *Asparagus cochinchinensis* (Lour.) Merr regulates macrophage immune response and epigenetic memory through TLR4-JNK/p38/ERK signaling pathway and histone modification. *Phytomedicine* **2024**, *124*, 155294. [CrossRef]
9. Zhan, X.; Xu, X.; Zhang, P.; Wang, X.; Hu, Z.; Zhao, W.; Hang, T.; Song, M. Crude polysaccharide from Danggui Buxue decoction enhanced the anti-tumor effect of gemcitabine by remodeling tumor-associated macrophages. *Int. J. Biol. Macromol.* **2023**, *242*, 125063. [CrossRef]
10. Li, Y.; Liu, Z.; Yan, H.; Zhou, T.; Zheng, L.; Wen, F.; Guo, G.; Zhang, Z. *Polygonatum sibiricum* polysaccharide ameliorates skeletal muscle aging and mitochondrial dysfunction via PI3K/Akt/mTOR signaling pathway. *Phytomedicine* **2025**, *136*, 156316. [CrossRef]
11. Bai, L.; Xu, D.; Zhou, Y.-M.; Zhang, Y.-B.; Zhang, H.; Chen, Y.-B.; Cui, Y.-L. Antioxidant Activities of Natural Polysaccharides and Their Derivatives for Biomedical and Medicinal Applications. *Antioxidants* **2022**, *11*, 2491. [CrossRef]
12. Pan, Y.; Luo, X.; Gong, P. *Spatholobi caulis*: A systematic review of its traditional uses, chemical constituents, biological activities and clinical applications. *J. Ethnopharmacol.* **2023**, *317*, 116854. [CrossRef]
13. Peng, F.; Hong, W.; Wang, Y.; Peng, Y.; Fang, Z. Mechanism of herb pair containing Astragali Radix and *Spatholobi caulis* in the treatment of myelosuppression based on network pharmacology and experimental investigation. *J. Ethnopharmacol.* **2024**, *319*, 117178. [CrossRef]
14. Liu, X.Y.; Xu, W.; Yang, X.W.; Zhang, P.; Zhao, W.; Gong, Y.; Liu, N.F. Study on non-flavonoids chemical constituents from *Spatholobi caulis*. *China J. Chin. Mater. Med.* **2020**, *45*, 1120–1127.
15. Zhang, Y.; Guo, L.; Duan, L.; Dong, X.; Zhou, P.; Liu, E.H.; Li, P. Simultaneous determination of 16 phenolic constituents in *Spatholobi caulis* by high performance liquid chromatography/electrospray ionization triple quadrupole mass spectrometry. *J. Pharm. Biomed. Anal.* **2015**, *102*, 110–118. [CrossRef]
16. Wang, Z.; Cai, T.; He, X. Characterization sulfated modification bioactivity of a novel polysaccharide from *Millettia dielsiana*. *Int. J. Biol. Macromol.* **2018**, *117*, 108–115. [CrossRef]

17. Chen, X.; Bahramimehr, F.; Shahhamzehei, N.; Fu, H.; Lin, S.; Wang, H.; Li, C.; Efferth, T.; Hong, C. Anti-aging effects of medicinal plants and their rapid screening using the nematode *Caenorhabditis elegans*. *Phytomedicine* **2024**, *129*, 155665. [CrossRef]
18. Zhang, H.; Pan, N.; Xiong, S.; Zou, S.; Li, H.; Xiao, L.; Cao, Z.; Tunnacliffe, A.; Huang, Z. Inhibition of polyglutamine-mediated proteotoxicity by Astragalus membranaceus polysaccharide through the DAF-16/FOXO transcription factor in *Caenorhabditis elegans*. *Biochem. J.* **2011**, *441*, 417–424. [CrossRef]
19. Li, H.; Shi, R.; Ding, F.; Wang, H.; Han, W.; Ma, F.; Hu, M.; Ma, C.W.; Huang, Z. Astragalus Polysaccharide Suppresses 6-Hydroxydopamine-Induced Neurotoxicity in *Caenorhabditis elegans*. *Oxidative Med. Cell. Longev.* **2016**, *016*, 4856761. [CrossRef]
20. Lin, C.; Su, Z.; Luo, J.; Jiang, L.; Shen, S.; Zheng, W.; Gu, W.; Cao, Y.; Chen, Y. Polysaccharide extracted from the leaves of *Cyclocarya paliurus* (Batal.) Iljinskaja enhanced stress resistance in *Caenorhabditis elegans* via *skn-1* and *hsf-1*. *Int. J. Biol. Macromol.* **2020**, *143*, 243–254. [CrossRef]
21. Peng, H.H.; Wu, C.Y.; Hsiao, Y.C.; Martel, J.; Ke, P.Y.; Chiu, C.Y.; Liau, J.C.; Chang, I.T.; Su, Y.H.; Ko, Y.F.; et al. Ganoderma lucidum stimulates autophagy-dependent longevity pathways in *Caenorhabditis elegans* and human cells. *Aging* **2021**, *13*, 13474–13495. [CrossRef]
22. Feng, S.; Cheng, H.; Xu, Z.; Feng, S.; Yuan, M.; Huang, Y.; Liao, J.; Ding, C. Antioxidant and anti-aging activities and structural elucidation of polysaccharides from *Panax notoginseng* root. *Process Biochem.* **2019**, *78*, 189–199. [CrossRef]
23. Zhang, X.; Chen, Q.; Chen, L.; Chen, X.; Ma, Z. Anti-Aging in *Caenorhabditis elegans* of Polysaccharides from *Polygonatum cyrtonema* Hua. *Molecules* **2024**, *29*, 1276. [CrossRef]
24. Liu, M.; Li, N.; Lu, X.; Shan, S.; Gao, X.; Cao, Y.; Lu, W. Sweet tea (*Rubus suavissmus* S. Lee) polysaccharides promote the longevity of *Caenorhabditis elegans* through autophagy-dependent insulin and mitochondrial pathways. *Int. J. Biol. Macromol.* **2022**, *207*, 883–892. [CrossRef]
25. Ferreira, S.S.; Passos, C.P.; Madureira, P.; Vilanova, M.; Coimbra, M.A. Structure–function relationships of immunostimulatory polysaccharides: A review. *Carbohydr. Polym.* **2015**, *132*, 378–396. [CrossRef]
26. Yang, J.; Song, Y.; Yu, Y.; Yang, X.; Zhang, X.; Zhang, W. Research progress on extraction techniques, structure-activity relationship, and biological functional mechanism of berry polysaccharides: A review. *Int. J. Biol. Macromol.* **2024**, *282*, 137155. [CrossRef]
27. Fu, Y.; Jiao, H.; Sun, J.; Okoye, C.O.; Zhang, H.; Li, Y.; Lu, X.; Wang, Q.; Liu, J. Structure-activity relationships of bioactive polysaccharides extracted from macroalgae towards biomedical application: A review. *Carbohydr. Polym.* **2024**, *324*, 121533. [CrossRef]
28. Wang, B.; Yan, L.; Guo, S.; Wen, L.; Yu, M.; Feng, L.; Jia, X. Structural Elucidation, Modification, and Structure-Activity Relationship of Polysaccharides in Chinese Herbs: A Review. *Front. Nutr.* **2022**, *9*, 908175. [CrossRef]
29. Kokoulin, M.S.; Kuzmich, A.S.; Romanenko, L.A.; Chikalovets, I.V. Sulfated capsular polysaccharide from the marine bacterium *Kangiella japonica* inhibits T-47D cells growth in vitro. *Carbohydr. Polym.* **2022**, *290*, 119477. [CrossRef]
30. Yu, S.; Ji, H.; Dong, X.; Liu, A.; Yu, J. FAS/FAS-L-mediated apoptosis autophagy of SPC-A-1 cells induced by water-soluble polysaccharide from *Polygala tenuifolia*. *Int. J. Biol. Macromol.* **2020**, *150*, 449–458. [CrossRef]
31. Song, W.; Jiang, S.; Chen, Y.; Chen, W.; Sun, L. Linking structure to solubility-related properties: Comprehensive characterization of polysaccharides from *Chaenomeles speciosa* (Sweet) Nakai. *Int. J. Biol. Macromol.* **2026**, *376*, 153603. [CrossRef]
32. Pettolino, F.A.; Walsh, C.; Fincher, G.B.; Bacic, A. Determining the polysaccharide composition of plant cell walls. *Nat. Protoc.* **2012**, *7*, 1590–1607. [CrossRef]
33. Yao, H.-Y.-Y.; Wang, J.-Q.; Yin, J.-Y.; Nie, S.-P.; Xie, M.-Y. A review of NMR analysis in polysaccharide structure and conformation: Progress, challenge and perspective. *Food Res. Int.* **2021**, *143*, 110290. [CrossRef]
34. Blois, M.S. Antioxidant Determinations by the Use of a Stable Free Radical. *Nature* **1958**, *181*, 1199–1200. [CrossRef]
35. Furuhashi, T.; Sakamoto, K. Central nervous system promotes thermotolerance via FoxO/DAF-16 activation through octopamine and acetylcholine signaling in *Caenorhabditis elegans*. *Biochem. Biophys. Res. Commun.* **2016**, *472*, 114–117. [CrossRef]
36. Chang, S.M.; Franklin, L.P.; Sattar, S.; Moro, C.A.; DeGennaro, M.V.; LaGanke, N.G.; Hanna-Rose, W. Mitochondrial sirtuins *sir-2.2* and *sir-2.3* regulate lifespan in *C. elegans*. *Genetics* **2025**, *231*, iyaf185. [CrossRef]
37. Naß, J.; Abdelfatah, S.; Efferth, T. The triterpenoid ursolic acid ameliorates stress in *Caenorhabditis elegans* by affecting the depression-associated genes *skn-1* and *prdx2*. *Phytomedicine* **2021**, *88*, 153598. [CrossRef]
38. Stuhr, N.L.; Nhan, J.D.; Hammerquist, A.M.; Van Camp, B.; Reoyo, D.; Curran, S.P. Rapid Lipid Quantification in *Caenorhabditis elegans* by Oil Red O and Nile Red Staining. *Bio-Protocol* **2022**, *12*, e4340. [CrossRef]
39. Leroy, M.; Mosser, T.; Manière, X.; Alvarez, D.F.; Matic, I. Pathogen-induced *Caenorhabditis elegans* developmental plasticity has a hormetic effect on the resistance to biotic and abiotic stresses. *BMC Evol. Biol.* **2012**, *12*, 187. [CrossRef]
40. Furuhashi, T.; Sakamoto, K. FoxO/Daf-16 restored thrashing movement reduced by heat stress in *Caenorhabditis elegans*. *Comp. Biochem. Physiol. B Biochem. Mol. Biol.* **2014**, *170*, 26–32. [CrossRef]
41. Gao, Y.-X.; Hu, S.-W.; Wang, N.; Wang, S.-Y.; Liu, N.; Li, X.-Q.; Duan, Q.-M.; Qi, Y.-C.; Cao, W. Structure characteristics of a pectic polysaccharide from the leaves of *Cornus officinalis* Sieb. et Zucc. (Shanzhuyu) and its inhibition on hepatocellular carcinoma. *Carbohydr. Polym.* **2026**, *376*, 124822. [CrossRef]

42. Xing, X.; Cui, S.W.; Nie, S.; Phillips, G.O.; Goff, H.D.; Wang, Q. Study on Dendrobium officinale O-acetyl-glucomannan (Dendronan®): Part II. Fine structures of O-acetylated residues. *Carbohydr. Polym.* **2015**, *117*, 422–433. [CrossRef]
43. Yuan, Q.; Zhang, X.; Ma, M.; Long, T.; Xiao, C.; Zhang, J.; Liu, J.; Zhao, L. Immunoenhancing glucuronoxylomannan from *Tremella aurantialba* Bandoni et Zang and its low-molecular-weight fractions by radical depolymerization: Properties, structures and effects on macrophages. *Carbohydr. Polym.* **2020**, *238*, 116184. [CrossRef]
44. Han, S.; Hu, F.; Ji, X.; Liu, Y.; Zhang, S.; Wang, Z.; Qiao, K. Polysaccharides from *Ziziphus jujuba* prolong lifespan and attenuate oxidative stress in *Caenorhabditis elegans* via DAF-16 and SKN-1. *Int. J. Biol. Macromol.* **2024**, *282*, 137482. [CrossRef]
45. Wang, X.; Zhang, Z.; Zhou, H.; Sun, X.; Chen, X.; Xu, N. The anti-aging effects of *Gracilaria lemaneiformis* polysaccharide in *Caenorhabditis elegans*. *Int. J. Biol. Macromol.* **2019**, *140*, 600–604. [CrossRef]
46. Liu, Q.; Yi, Y.-L.; Liang, X.-F.; Wu, M.-T.; Li, J.; Chen, X.; Zhang, F.; Ruan, Q.-L.; Liu, F.; Duan, J.-A.; et al. Antioxidant and antiaging activities of the polysaccharide ZJP-04M from *Ziziphus jujuba* in *Caenorhabditis elegans*. *Int. J. Biol. Macromol.* **2025**, *284*, 138208. [CrossRef]
47. Chen, N.; Jiang, T.; Xu, J.; Xi, W.; Shang, E.; Xiao, P.; Duan, J.-A. The relationship between polysaccharide structure and its antioxidant activity needs to be systematically elucidated. *Int. J. Biol. Macromol.* **2024**, *270*, 132391. [CrossRef]
48. Wang, Z.; Zheng, Y.; Lai, Z.; Hu, X.; Wang, L.; Wang, X.; Li, Z.; Gao, M.; Yang, Y.; Wang, Q.; et al. Effect of monosaccharide composition and proportion on the bioactivity of polysaccharides: A review. *Int. J. Biol. Macromol.* **2024**, *254*, 127955. [CrossRef]
49. Wang, J.; Hu, S.; Nie, S.; Yu, Q.; Xie, M. Reviews on Mechanisms of In Vitro Antioxidant Activity of Polysaccharides. *Oxidative Med. Cell. Longev.* **2016**, *2016*, 5692852. [CrossRef]
50. Wei, N.; Wang, X.; Wu, Y.; Liu, L.; Zhao, Y.; Zhao, R. Comparative Study on Anti-Inflammatory Effect of Polysaccharides from Vinegar-Baked Radix Bupleuri Using Different Methods. *ACS Omega* **2023**, *8*, 29253–29261. [CrossRef]
51. Ma, R.; Cao, T.; An, H.; Yu, S.; Ji, H.; Liu, A. Extraction, purification, structure, and antioxidant activity of polysaccharide from *Rhodiola rosea*. *J. Mol. Struct.* **2023**, *1283*, 135310. [CrossRef]
52. Yang, M.; Zhou, D.; Xiao, H.; Fu, X.; Kong, Q.; Zhu, C.; Han, Z.; Mou, H. Mou, Marine-derived uronic acid-containing polysaccharides: Structures, sources, production, and nutritional functions. *Trends Food Sci. Technol.* **2022**, *122*, 1–12. [CrossRef]
53. Zhu, J.; Zhou, H.; Zhang, J.; Li, F.; Wei, K.; Wei, X.; Wang, Y. Valorization of Polysaccharides Obtained from Dark Tea: Preparation. Physicochemical. Antioxidant, and Hypoglycemic Properties. *Foods* **2021**, *10*, 2276. [CrossRef]
54. Šupljika, F.; Kovačević, M.; Semenčić, M.Č. Mushroom-Derived Compounds as Inhibitors of Advanced Glycation End-Products. *Appl. Sci.* **2026**, *16*, 617. [CrossRef]
55. Alias, A.H.D.; Rizal, I.S.A.M.; Yusof, M.A.; Radzi, M.R.M.; Shafie, M.H. Extraction technologies and structural elucidation of polysaccharides from herbs and spices: Connecting molecular characteristics to biofunctional properties. *Carbohydr. Res.* **2026**, *566*, 109963. [CrossRef]
56. Pak, U.; Cheng, H.; Liu, X.; Wang, Y.; Ho, C.; Ri, H.; Xu, J.; Qi, X.; Yu, H. Structural characterization and anti-oxidation activity of pectic polysaccharides from *Swertia mileensis*. *Int. J. Biol. Macromol.* **2023**, *248*, 125896. [CrossRef]
57. Urias-Orona, V.; Huerta-Oros, J.; Carvajal-Millán, E.; Lizardi-Mendoza, J.; Rascón-Chu, A.; Gardea, A.A. Component analysis and free radicals scavenging activity of *Cicer arietinum* L. husk pectin. *Molecules* **2010**, *15*, 6948–6955. [CrossRef]
58. Wang, Q.; Wu, J.; Huang, J.; Yang, L.; Tao, J.; Nie, J.; Zhao, J.; Wang, Y.-N. *Cremastra appendiculata* polysaccharides improve stress resistance and prolong the lifespan of *Caenorhabditis elegans* via *daf-16* in the insulin signaling pathway. *Int. J. Biol. Macromol.* **2023**, *229*, 496–506. [CrossRef]
59. Lee, Q.; Xue, Z.; Zheng, M.; Liu, B.; Zeng, F. Antioxidant activity of low molecular weight polysaccharides from *Tremella fuciformis* in *Caenorhabditis elegans* based on metabolomics analysis. *J. Future Foods* **2026**, *6*, 479–490. [CrossRef]
60. Zhu, J.; Jia, Y.; Wang, C.; Zhou, W.; Shu, Y.; Zhang, K.; Zeng, X.; Guo, R. *Lonicera japonica* polysaccharides improve longevity and fitness of *Caenorhabditis elegans* by activating DAF-16. *Int. J. Biol. Macromol.* **2023**, *229*, 81–91. [CrossRef]

Disclaimer/Publisher's Note: The statements, opinions and data contained in all publications are solely those of the individual author(s) and contributor(s) and not of MDPI and/or the editor(s). MDPI and/or the editor(s) disclaim responsibility for any injury to people or property resulting from any ideas, methods, instructions or products referred to in the content.